Drift-controlled design of reinforced concrete frame structures under distant blast conditions—Part II: Implementation and evaluation

Bing Li*, Hai-Cheng Rong, Tso-Chien Pan

Protective Technology Research Center, Nanyang Technological University, 50 Nanyang Ave, Singapore 639798, Singapore

Abstract

The model for the calculation of an equivalent static force (ESF) and the design procedure with ESF for single-degree-of-freedom (SDOF) systems presented in the first part of the two-part paper are extended into the design for a reinforced concrete (RC) frame structure under distant blast conditions. An empirical formula for the ESF factor involved in the ESF model is presented based on sample points obtained by comparing the nonlinear dynamic responses of frame structures under the blast loading with the corresponding nonlinear pushover analysis of the structure due to an ESF. The use of the method is demonstrated with two six-storey RC frame structures. Numerical verification of the method indicates that the maximum inter-storey drift ratios (MIDR) of the two designed frame structures in comparison to their respective targets are conservative to some extent. The reasons that may lead to the conservative designs are discussed.

Keywords: Maximum inter-storey drift ratio; Equivalent static force; Reinforced concrete frame structure; Blast loading

1. Introduction

A design method based on an equivalent static force (ESF) is developed in the companion paper for a reinforced concrete (RC) frame structure in terms of controlling its maximum inter-storey drift ratio (MIDR), the ratio of maximum inter-storey drift to the storey height, under blast loading from a distant surface explosion. Four basic assumptions are made as follows:

(1) The MIDR can be treated as a reasonable and sufficient response parameter for the identification of structural global performance level, and the critical side-sway limits in term of inter-storey drift ratio as documented in an ASCE special publication [1] can properly reflect different performance levels for a frame structure.
(2) The MIDR will occur at a time later than the blast loading duration (t_d). Therefore, further response after t_d occurs as a result of transforming kinetic energy into strain energy of the structure. For most frame structures, this assumption is acceptable considering the relatively short duration t_d of the blast loading [2,3].

*Corresponding author.
E-mail address: cbli@ntu.edu.sg (B. Li).

(3) The nonlinear relationship between displacement and resistance of the frame structure under the action of the lateral forces can be reasonably idealized as an elastic-perfectly-plastic function. Consequently the calculated ESF will be the minimum required ultimate strength of the structural system based on which the reinforcement of the structure is designed.
(4) The model for calculation of ESF for a RC frame structure has a form similar to that for an elastic-perfectly-plastic single-degree-of-freedom (SDOF) system derived in the companion paper [4].

Based on the above assumptions, the process for the development of ESF for a SDOF system can be extended to a RC frame structure in term of vectors. However, there is a significant difference in the determination of the ESF factors through numerical studies compared to closed-form solutions. A simple empirical equation for the ESF factor is derived for the convenience of blast resistant design with ESF. For illustration and evaluation of the design method developed, two design examples are given for six-storey RC frame structures under different blast loadings followed by numerical verifications.

2. ESF for a RC frame structure

2.1. Process for the development of ESF

For a frame structure with n storeys, the ESF (P_{st}) is defined as a column vector of force, which, when applied statically to each floor level, can produce the same MIDR as that under a blast load, thus

$$P_{st} = \{P_{st,1}, P_{st,2}, \ldots, P_{st,n}\}^T, \tag{1}$$

where $P_{st,i}$ represents the component of ESF at the ith floor level. The process of P_{st} evaluation is shown in Fig. 1. At the end of the blast loading duration t_d, the frame structure responds with a distribution of displacement and velocity as shown in Fig. 1(a), where $y_{t_d} = \{y_{t_d,1}, y_{t_d,2}, \ldots, y_{t_d,n}\}^T$ and $y_{t_d,i}$ stands for the ith floor displacement at time t_d. With the increase in time, the distributed kinetic energy as a function of the velocity will be gradually transformed into further deformation reaching the MIDR (Δ_m). Therefore, if the kinetic energy $W_{k,i}$, which represents the kinetic energy within the part of the structure located halfway above and below the ith floor level at time t_d, is concentrated and represented by the strain energy $W_{a,i}$ of an additional uncoupled elastic spring $K_{a,i}$ at the corresponding floor level with the same deformation as $y_{t_d,i}$, an equivalent static system can be established in Fig. 1(b). For the additional uncoupled elastic spring, $W_{a,i}$ and $K_{a,i}$ can be obtained as

$$W_{a,i} = \tfrac{1}{2}K_{a,i}, \quad y_{t_d,i}^2 = W_{k,i}, \tag{2}$$

$$K_{a,i} = \frac{2W_{k,i}}{y_{t_d,i}^2}, \tag{3}$$

where $K_{a,i}$ is the stiffness of the additional elastic spring at the ith floor level. According to the equilibrium of the equivalent static system, the external static force ($P = \{P_1, P_2, \ldots, P_n\}^T$) will include two parts: the first one is the resistive force of the frame structure ($F_s = \{F_{s,1}, F_{s,2}, \ldots, F_{s,n}\}^T$) corresponding to the deformation of y_{t_d} and the second part of the force ($F_a = \{F_{a,1}, F_{a,2}, \ldots, F_{a,n}\}^T$) which is associated with the additional springs, thus

$$P = F_s + F_a, \tag{4}$$

where $F_{a,i}$ for the additional elastic spring at the deformation of $y_{t_d,i}$ is given as

$$F_{a,i} = K_{a,i} y_{t_d,i}. \tag{5}$$

Substituting Eq. (3) into (5) produces

$$F_{a,i} = \frac{2W_{k,i}}{y_{t_d,i}}. \tag{6}$$

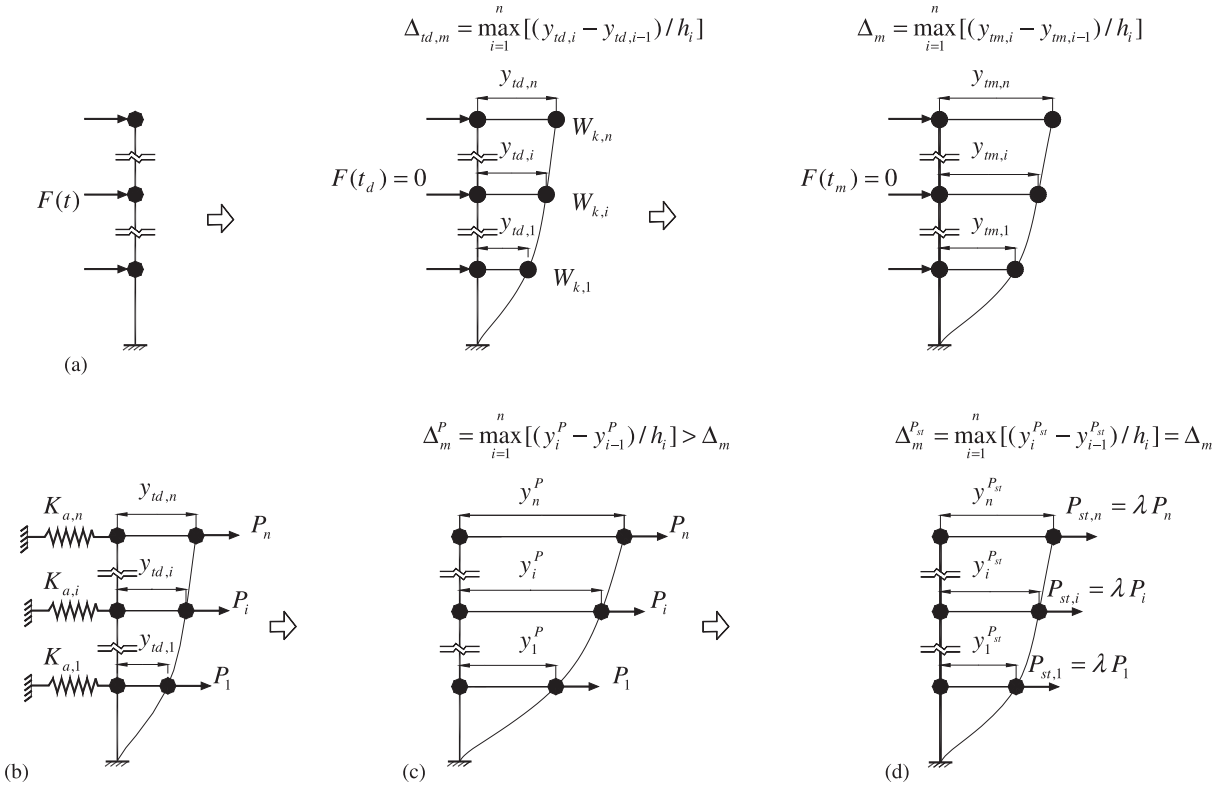

Fig. 1. Process for the construction of ESF for a RC frame structure. (a) Dynamic response under the blast force; (b) equivalent static system; (c) static responses under P; (d) static responses under P_{st}.

In order to simulate the transformation of the kinetic energy into further deformation after t_d, the strain energy within the springs $K_{a,1}, K_{a,2}, \ldots, K_{a,n}$ is statically released in such a manner that their supports move towards the springs until the equivalent static system reverts to the original frame structure with P acting on it. However, when considering the extra positive external work produced by P together with the declining reaction force of the springs at their supports during the energy transformation process, a larger MIDR will be induced in this way than that of the frame structure under the blast loading (Δ_m) as shown in Fig. 1(c). Thus, an ESF factor λ is introduced to decrease P so as to produce the ESF (P_{st}), which creates the same MIDR as Δ_m when statically applied to the original frame structure as illustrated in Fig. 1(d)

$$P_{st} = \lambda P. \tag{7}$$

2.2. ESF factor

For a RC frame structure under the blast condition, it is difficult to derive a closed-form expression for λ such as that in the companion paper [4]. An empirical formula developed by numerical studies seems to be a practical solution. If a number of sample points (the accurate values of λ for different frame structures under various blast loadings) are available, an empirical formula can be found with an unconstraint nonlinear optimization technique, which finds the minimum of a scalar function of several variables starting at an initial estimate. Therefore, two main operations are performed in the determination of the ESF factor formula; to get reliable sample points of λ, and establish such a formula.

2.2.1. Sample points of the ESF factor

The sample point of λ is obtained by comparing the MIDR of a RC frame structure under a blast loading with the corresponding nonlinear static pushover analysis result of the structure under the force P. In this

pushover analysis the magnitude of the structural loading is incrementally applied in accordance with a certain predefined pattern of the lateral load vector P. The procedures are listed in the following:

1. Establish a frame structure and a blast loading acting on it.
2. Evaluate $y_{t_d,i}$, $W_{k,i}$ and Δ_m, the MIDR within the whole dynamic response process, with numerical dynamic simulation.
3. Calculate the recovery force $F_{a,i}$ by applying $y_{t_d,i}$ to the structure through nonlinear static analysis.
4. Compute the external static force P with Eqs. (4) and (6).
5. Carry out the nonlinear pushover analysis of the frame structure under a gradually increasing load vector distributed as P.
6. Plot the curves obtained for load versus the inter-storey drift responses for different storey levels, and find the value of λ at the critical storey level whose inter-storey drift ratio firstly reaches the value of Δ_m under the gradually increasing force of P (Fig. 2).

Sixty sample points of λ are evaluated by using the above procedures, where four different planar frame structures are subjected to a variety of lateral blast pressures uniformly applied to the exterior columns plus the service loads uniformly distributed along the beams (F_{ser}) in a vertical direction. Additional masses along with the beams (M_{add}) are involved that are contributed by the adjacent floors. The details of the frame structures and the analytical results for λ are shown in Tables 1 and 2, where $\Delta_{t_d,m}$ and Δ_m represent the MIDR of the structure at time t_d of the blast loading and the MIDR during the whole dynamic response range, respectively. The dynamic analysis of the frame structure under the blast loading to find $\Delta_{t_d,m}$ and Δ_m are obtained using the nonlinear finite element analyses with the ABAQUS software [5,6]. The software is also utilized for the nonlinear static analysis of the structure under the gradually increasing force of P to further obtain the value of λ. The concrete model is employed to represent the concrete properties, which uses concepts of smeared cracking in the sense that it does not track individual "macro" cracks and isotropic compressive plasticity to represent the inelastic behaviour of concrete. Reinforcement is simulated by the Von-Mises yield criterion with associated flow and isotropic strain hardening. Furthermore, Timoshenko beam elements are used for the beams and columns while shell elements are for the modelling of floor slabs. The reinforcement is placed at its exact location by the rebar option in ABAQUS. The finite element models have been verified from a simply supported beam and a square slab subjected to blast loading where numerically predicted responses have a good match with experimental ones [7].

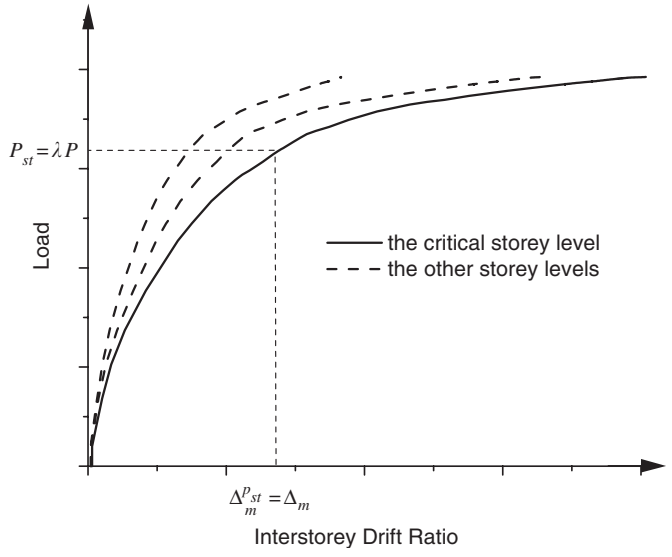

Fig. 2. Nonlinear pushover analysis under a gradually increasing lateral force vector distributed as P

Table 1
Different frame structures involved in the determination of sample points of λ

Structural type	Storey level	Height (mm)	Width (mm)	Column section (mm × mm)	Beam section (mm × mm)	Column reinforcement Ratio[a] (%)	Beam reinforcement ratio[b] (%)		
							End section	Mid-span section	Interior support
I-1	1–2 3–6	4500 3300	3 × 6000	600 × 600 500 × 500	300 × 600	1.5	1.1/0.5	0.5/0.8	1.1/0.5
I-2	1–2 3–6	4500 3300	3 × 6000	700 × 700 600 × 600	300 × 700	1.1	0.9/0.4	0.3/0.6	0.9/0.4
II	1–4	3600	3 × 5400	500 × 500	300 × 500	2.0	1.5/0.7	0.6/1.2	1.5/0.7
III	1–2 3–9	4500 3300	3 × 6000	800 × 800 700 × 700	300 × 700	1.0	0.8/0.5	0.3/0.6	0.8/0.5

Material properties: concrete dynamic compressive strength of 40 MPa; longitudinal reinforcement dynamic yield strength of 520 MPa.
[a]Total reinforcement ratio in the cross-section of the columns where the tension and compression reinforcements are equal.
[b]The upper/lower longitudinal reinforcement for the beam cross-section.

2.2.2. Formulae of the ESF factor

Since it is assumed that the relationship of λ with $\Delta_{t_d,m}$ and Δ_m follows a form similar to that for a SDOF system, λ can be written as

$$\lambda = AX + B,$$
$$X_j = \begin{cases} \Delta_{t_d,m}/\Delta_m, & \Delta_m \leqslant a, \\ \Delta_{t_d,m}/(2\Delta_m - a), & \Delta_{t_d,m} \leqslant a \text{ and } \Delta_m \geqslant a, \\ \Delta_{t_d,m}/(2\Delta_m - \Delta_{t_d,m}), & \Delta_{t_d,m} \geqslant a. \end{cases} \tag{8}$$

Two factors that should be acknowledged are listed: (i) the value of λ is determined by the relationship of lateral load versus the inter-storey drift response of the frame structure, which is a continuously curved function; (ii) the process of releasing the kinetic energy into further deformation after t_d for a frame structure under the blast condition is more complicated than the process of releasing the strain energy of the additional springs in the equivalent static system. As a consequence, A, B and a in Eq. (8) are defined to be three uncertain parameters whose values are determined in such a manner that Eq. (8) could make the closest predictions of the available sample points of λ. In terms of mathematics, it can be expressed with the following optimum model

$$\text{find}: \ A, B \text{ and } a$$
$$\text{minimize}: \ \Phi = \sum_{j=1}^{m} [\lambda_{\text{samp},j} - \lambda_j]^2$$
$$\text{subject to } \lambda_j = AX_j - B$$
$$X_j = \begin{cases} \Delta^j_{t_d,m}/\Delta^j_m, & \Delta^j_m \leqslant a, \\ \Delta^j_{t_d,m}/(2\Delta^j_m - a), & \Delta^j_{t_d,m} \leqslant a \text{ and } \Delta^j_m \geqslant a, \\ \Delta^j_{t_d,m}/(2\Delta^j_m - \Delta^j_{t_d,m}), & \Delta^j_{t_d,m} \geqslant a, \end{cases} \tag{9}$$

where $\lambda_{\text{samp},j}$, $\Delta^j_{t_d,m}$ and Δ^j_m indicate the jth sample point of the ESF factor, the corresponding MIDR at time t_d and that during the whole response process as listed in Table 2, λ_j is the predicted value of the ESF factor according to Eq. (8).

Table 2
Sixty different cases in the determination of sample points of λ

Case	Structural type	P_r (kPa)[a]	t_d (ms)	F_{ser} (kN/m)	M_{add} (kg/m)	$\Delta_{t_d,m}$(%)	Δ_m (%)	λ
1	I-1	434	42.8	60	No	0.488	2.301	0.160
2	I-1	434	42.8	No	No	0.594	2.811	0.129
3	I-1	217	42.8	60	No	0.258	0.878	0.230
4	I-1	217	42.8	No	No	0.252	0.964	0.169
5	I-1	200	30.0	60	No	0.125	0.517	0.226
6	I-1	200	30.0	No	No	0.141	0.564	0.255
7	I-1	300	30.0	60	No	0.191	0.844	0.201
8	I-1	300	30.0	No	No	0.222	0.978	0.232
9	I-1	400	30.0	60	No	0.257	1.216	0.170
10	I-1	400	30.0	No	No	0.311	1.516	0.193
11	I-1	500	30.0	60	No	0.335	1.743	0.160
12	I-1	500	30.0	No	No	0.408	2.101	0.162
13	I-1	100	30.0	60	No	0.061	0.203	0.272
14	I-1	700	30.0	60	No	0.499	2.855	0.124
15	I-1	100	35.0	60	No	0.077	0.303	0.247
16	I-1	200	50.0	60	No	0.290	1.051	0.301
17	I-2	200	50.0	60	No	0.222	0.661	0.319
18	I-1	200	50.0	60	2700	0.164	0.517	0.400
19	I-1	300	50.0	60	No	0.453	1.970	0.256
20	I-2	300	50.0	60	No	0.338	1.233	0.260
21	I-1	300	50.0	60	2700	0.260	0.861	0.345
22	I-1	400	50.0	60	No	0.655	3.093	0.211
23	I-2	400	50.0	60	No	0.435	1.953	0.215
24	I-1	400	50.0	60	2700	0.366	1.240	0.236
25	I-1	500	50.0	60	No	0.888	4.478	0.169
26	I-2	500	50.0	60	No	0.576	2.845	0.168
27	I-1	500	50.0	60	2700	0.474	1.584	0.271
28	I-1	200	60.0	60	No	0.406	1.361	0.244
29	I-1	200	60.0	60	2700	0.180	0.641	0.199
30	I-1	300	60.0	60	No	0.608	2.532	0.192
31	I-1	300	60.0	60	2700	0.296	1.171	0.199
32	I-1	400	60.0	60	No	0.887	4.068	0.147
33	I-1	400	60.0	60	2700	0.434	1.784	0.187
34	I-1	150	60.0	60	No	0.302	0.882	0.331
35	I-1	150	60.0	60	2700	0.126	0.451	0.196
36	II	434	42.8	54	2880	0.377	1.484	0.152
37	II	300	42.8	54	2880	0.258	0.944	0.185
38	II	200	42.8	54	2880	0.166	0.582	0.183
39	II	800	42.8	54	2880	0.719	3.156	0.144
40	II	600	42.8	54	2880	0.519	2.255	0.142
41	II	300	60.0	54	2880	0.371	1.329	0.255
42	II	200	60.0	54	2880	0.231	0.780	0.251
43	II	600	60.0	54	2880	0.875	3.307	0.237
44	II	800	60.0	54	2880	1.243	5.167	0.229
45	II	500	50.0	54	2070	0.657	2.349	0.341
46	II	600	50.0	54	2070	0.825	3.100	0.317
47	II	700	50.0	54	2070	1.003	3.992	0.294
48	II	600	35.0	54	2070	0.467	2.081	0.137
49	II	800	35.0	54	2070	0.636	2.875	0.124
50	II	900	42.8	54	2475	0.656	2.630	0.130
51	III	434	42.8	60	3150	0.156	0.758	0.127
52	III	600	42.8	60	3150	0.229	1.206	0.084
53	III	500	42.8	60	3150	0.183	0.930	0.106
54	III	300	42.8	60	3150	0.105	0.475	0.196
55	III	500	60.0	60	3150	0.296	1.574	0.149
56	III	700	60.0	60	3150	0.486	2.962	0.129
57	III	500	60.0	60	2100	0.346	1.998	0.090

Table 2 (*continued*)

Case	Structural type	P_r (kPa)[a]	t_d (ms)	F_{ser} (kN/m)	M_{add} (kg/m)	$\Delta_{t_d,m}$(%)	Δ_m (%)	λ
58	III	300	60.0	60	2100	0.168	0.861	0.112
59	III	500	50.0	60	3360	0.345	1.688	0.149
60	III	300	50.0	60	3360	0.187	0.792	0.153

[a] P_r, blast peak pressure.

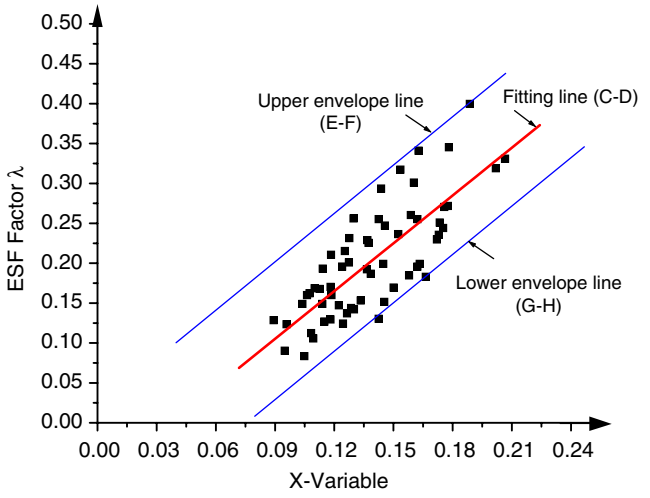

Fig. 3. Distribution of sample points of the ESF factors and the optimum fitting curve.

Many available algorithms can be applied for solving such an optimum problem. In this study, a direct search method [8] provided in the function 'Fminsearch' of MATLAB [9], is utilized for optimal solution of Eq. (9). The results are plotted in Fig. 3, where $A \approx 1.996$, $B \approx -0.074$ and $a \approx 0$, and the line C–D indicates the optimized $\lambda - X$ function. It can be seen in Fig. 3 that the sample points of λ_{samp} are scattered around this optimized function within a straight strip bounded between an upper-envelope (E–F) and a lower-envelope line (G–H). By substituting the optimum results of the parameters A, B and a into Eq. (8), the line C–D can be written as

$$\lambda = 1.996X - 0.074,$$
$$X = \Delta_{t_d,m}/(2\Delta_m - \Delta_{t_d,m}). \tag{10}$$

The lines E–F and G–H are expressed, respectively, as

$$\lambda_{upp} = 1.996X + 0.023,$$
$$X = \Delta_{t_d,m}/(2\Delta_m - \Delta_{t_d,m}) \tag{11}$$

and

$$\lambda_{low} = 1.996X - 0.160,$$
$$X = \Delta_{t_d,m}/(2\Delta_m - \Delta_{t_d,m}). \tag{12}$$

3. Design of a reinforced concrete frame structure with the ESF

Similar to the trend of ultimate strength with the maximum displacement for a SDOF system, if the resistance of a frame structure between its inter-storey drift ratio at the critical storey level and an increasing

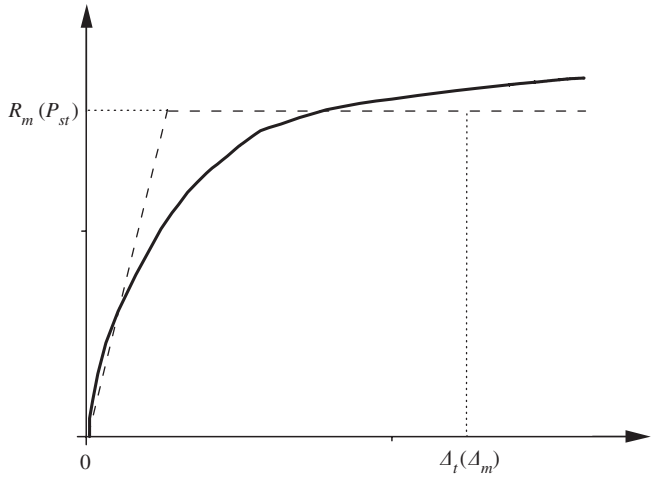

Fig. 4. Elastic-perfectly-plastic function of ultimate strength versus inter-storey drift ratio at the critical storey level.

lateral load vector distributed as P can be idealized as an elastic-perfectly-plastic function, the MIDR of the structure under the blast condition is closely related to the ultimate strength R_{m} as shown in Fig. 4. With a predefined target MIDR denoted as Δ_{t}, the required R_{m} of the structure should be equal to the ESF (P_{st}) predicted according to the previous process by taking its MIDR Δ_{m} as Δ_{t}, which can be applied to determine the reinforcement after giving the dimension of the frame members.

The required R_{m} (P_{st}) is predicted from the product of P with the ESF factor λ. Although Eq. (10) can provide an optimum value for λ, it may in some situations result in an inadequate estimation of R_{m}. For the purpose of design, considering the safety of the frame structure, the conservative upper-envelop line (E–F) is suggested. Therefore, by combining Eqs. (4), (7) and (11) and replacing P_{st} and Δ_{m} with R_{m} and Δ_{t}, respectively, the following is obtained:

$$R_{\mathrm{m}} = \lambda_{\mathrm{upp}} P, \quad P = F_{\mathrm{s}} + F_{\mathrm{a}},$$
$$\lambda_{\mathrm{upp}} = 1.996X + 0.023, \quad X = \Delta_{t_{\mathrm{d}},\mathrm{m}}/(2\Delta_t - \Delta_{t_{\mathrm{d}},\mathrm{m}}). \tag{13}$$

With Eq. (13), the blast resistant design using the ESF is iteratively accomplished as follows. According to the expected performance level for the frame structure, a target MIDR Δ_t is defined at the start of the design. Giving the dimensions of different structural members and the initial reinforcement ratios ρ_0, the required R_{m} is obtained from Eq. (13), which together with service loadings will produce new reinforcement ratios ρ_1. Hence, make $\rho_0 = \rho_1$ and repeat the above steps until convergence of reinforcement ratios is reached.

There exists the possibility that the cross-sectional sizes of structural members are specified to be unreasonably small during the design stage. With the above iterative design procedures, the reinforcement ratios could be determined as well. However they might exceed the allowable maximum value. In such cases, modifications to the cross-sectional sizes of the frame members are needed. The flowchart of the design procedure is shown in Fig. 5.

4. Illustrative examples

For illustration of the blast resistant design procedures developed with the ESF, two design examples are carried out for planar six-storey RC frame structures to resist blast loading from distant surface explosions as shown in Fig. 6. The blast loadings considered in these two design examples are actually related to the explosion of 80 t TNT at 100 m and 30 t TNT at 100 m when the blast loadings are simplified to be triangular. The hemispherical blast waves producing at about 100 m can be reasonably modelled with a planar wave applied nearly uniformly on the exposed surfaces of the six-storey RC frame structure. Based on the definition of the distant blast wave in the introduction of the companion paper [4], these blast events are distant relative to the six-storey frame structure analysed. The basic objective of the design is to ensure that the MIDR of the

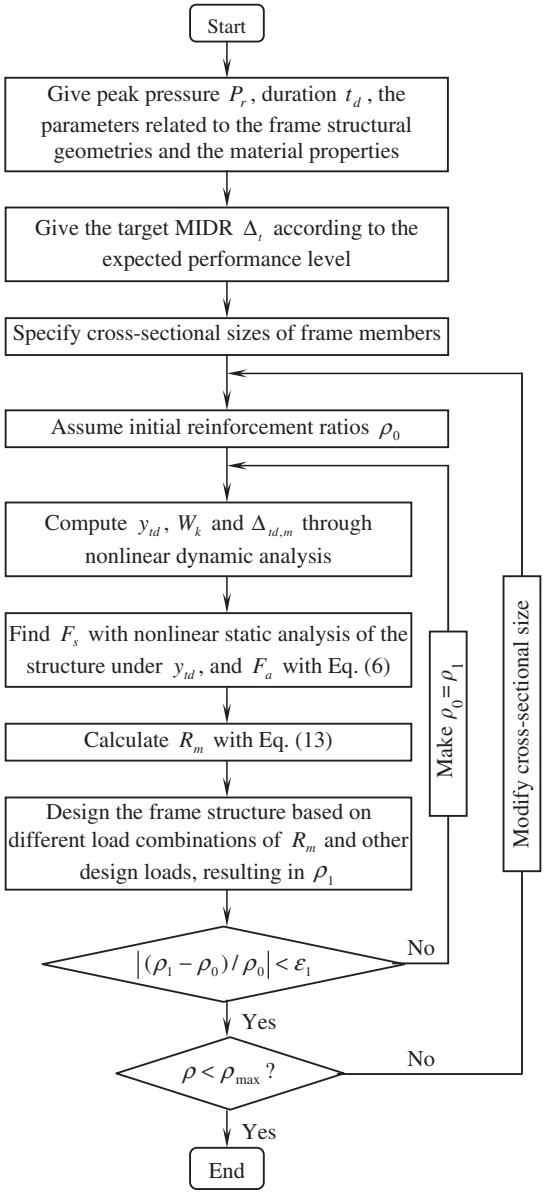

Fig. 5. Drift-controlled design flowchart of a RC frame structures based on ESF of a blast loading from distant explosion (ε^1 is an arbitrarily small value).

designed structural system is within the expected performance level defined by the target MIDR. Three types of external actions are considered within the design, which include the blast loads, the dead loads (DL) and live loads (LL). The blast loading consists of the net lateral pressures on the exterior columns and vertical roof pressures. However, as discussed in previous research [10], the vertical roof pressures have a slight effect on the frame sidesway response and are therefore ignored in these examples. The consideration of the vertical roof loadings can be involved in the blast resistant design of structural members including the floor slabs and the roof beams with appropriate design guidance [11,12]. The detailed loading profiles are displayed in Fig. 6, where DL = 30 kN/m and LL = 24 kN/m.

In the first design example, a low performance level is required for the frame structure, accordingly a relatively large target MIDR of $\Delta_t = 3.5\%$ is given which is slightly less than the drift limit (4%)

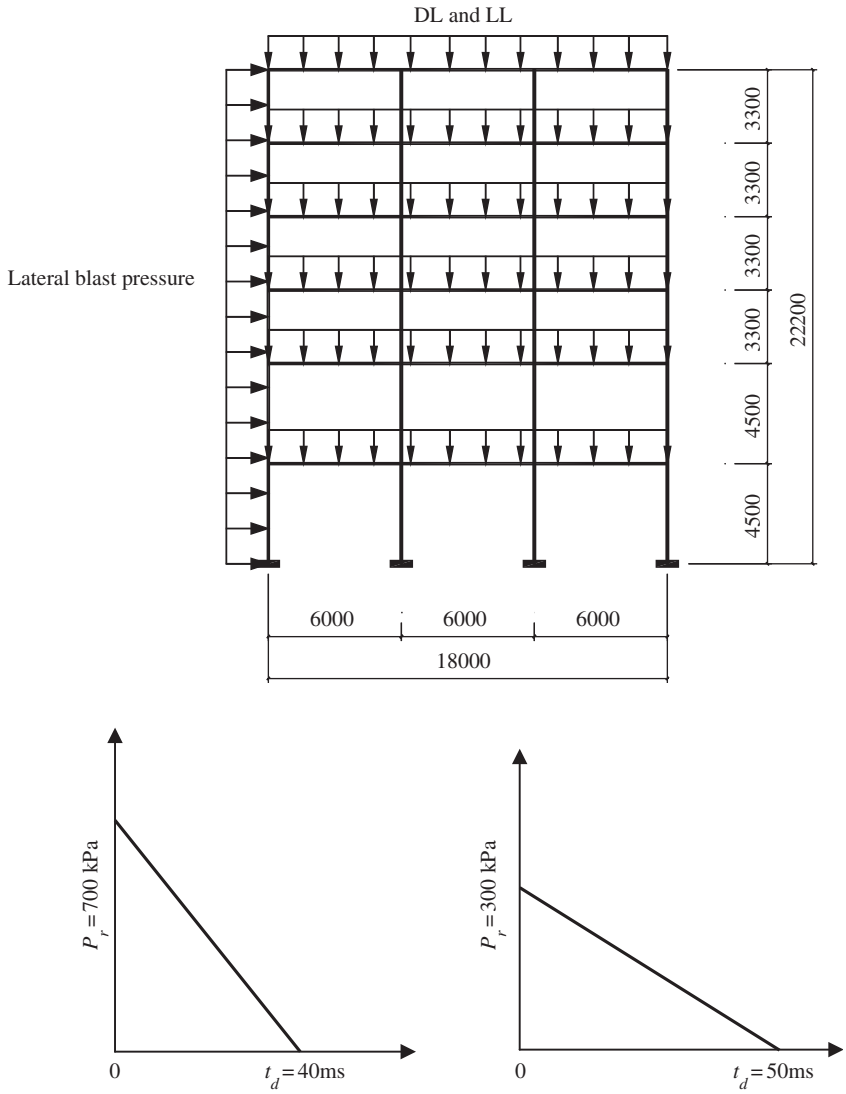

Fig. 6. A six-storey RC frame structure under blast forces (Examples I and II) unit: mm. I: net lateral blast pressure, II: net lateral blast pressure.

corresponding to the state that the structure may lose its integrity or even collapse as listed in the ASCE special publication [1]. In the second example, a high performance level is expected for the frame structure to resist the blast loading, and thus a lower target MIDR of $\Delta_t = 1.5\%$ is defined.

At the start of design, the cross-sectional sizes for frame members are specified to be 600 mm × 600 mm for the columns in the first and second storeys, 500 mm × 500 mm for the other columns and 300 mm × 600 mm for all frame beams. Giving the initial values for reinforcement ratios ρ_0, R_m is computed at each iterative step from Eq. (12). The determination of ρ_1 is accomplished with the integrated building design software ETABS [13] according to four user-specified loading combinations (1.4DL + 1.6LL + 1.0R_m, 1.4DL + 1.6LL−1.0R_m, 1.4DL + 1.6LL and 1.4DL).

The whole design procedures for these two design examples with the method based on ESF presented in this paper are listed in Tables 3 and 4, where the convergence condition is defined as $|(\rho_1 - \rho_0)/\rho_0| \leqslant 0.05$. It can be observed that convergence with ESF is rapid, as only three iterative steps are needed for both design examples.

Although nonlinear dynamic analysis is needed to find y_{t_d} and W_k at each step, little computational time is consumed to accomplish this analysis since only slight nonlinear behaviour of frame structure is apparent at time t_d due to the short duration of blast loading. Moreover, the reinforcement ratios obtained for the members are all located in their suitable ranges. Hence, there is no need for a change to the initially specified cross-sectional sizes of the frame members.

5. Numerical verification of the design method

To check whether the MIDR is controlled effectively when the above design method is implemented, nonlinear finite element analyses are performed on the frame structures designed against the given blast forces. Two steps of analysis are involved in which the nonlinear static analysis under the combined effect of DL and LL is first carried out followed by the nonlinear dynamic analysis of the designed structures under the blast force. The simulation results are demonstrated in Figs. 7 and 8, which show a conservative MIDR at 1.31% and 0.72%, respectively, for these two frames as compared to the respective target MIDR.

The reasons for the conservative design with ESF can be explained in two ways. Firstly, the prediction of the ESF factor λ based on its upper-envelope line induces an overestimation of R_m from Eq. (12). The second relies on the assumption that the resistance of the designed structure is an elastic-perfectly-plastic function and therefore the calculated ESF will be equal to the required R_m. The strength hardening of the structure which exceeded the value of R_m as shown in Fig. 4 is not considered in the design procedure. From the viewpoint of structural safety, such a conservative design result can be acceptable.

Table 3
Design procedures for example I

i	$y_{t_d,i}$ (mm) 2	$W_{k,i}$ (N m)	$F_{a,i}$ (N)	$F_{s,i}$ (N)	P_i (N)	$\Delta_{t_d,m}$ (%)	X	λ	$P_{st,i}$ (N)
The first iterative design step									
6	10.80	0.93×10^4	1.72×10^6	-3.91×10^5	1.33×10^6				2.09×10^5
5	19.25	1.73×10^4	1.80×10^6	3.99×10^5	2.20×10^6				3.45×10^5
4	20.40	2.48×10^4	2.43×10^6	0.11×10^5	2.44×10^6	0.441	0.067	0.157	3.84×10^5
3	20.77	2.80×10^4	2.69×10^6	-2.08×10^5	2.49×10^6				3.91×10^5
2	22.85	2.61×10^4	2.28×10^6	0.75×10^5	2.36×10^6				3.70×10^5
1	19.83	1.10×10^4	1.11×10^6	1.19×10^6	2.30×10^6				3.61×10^5

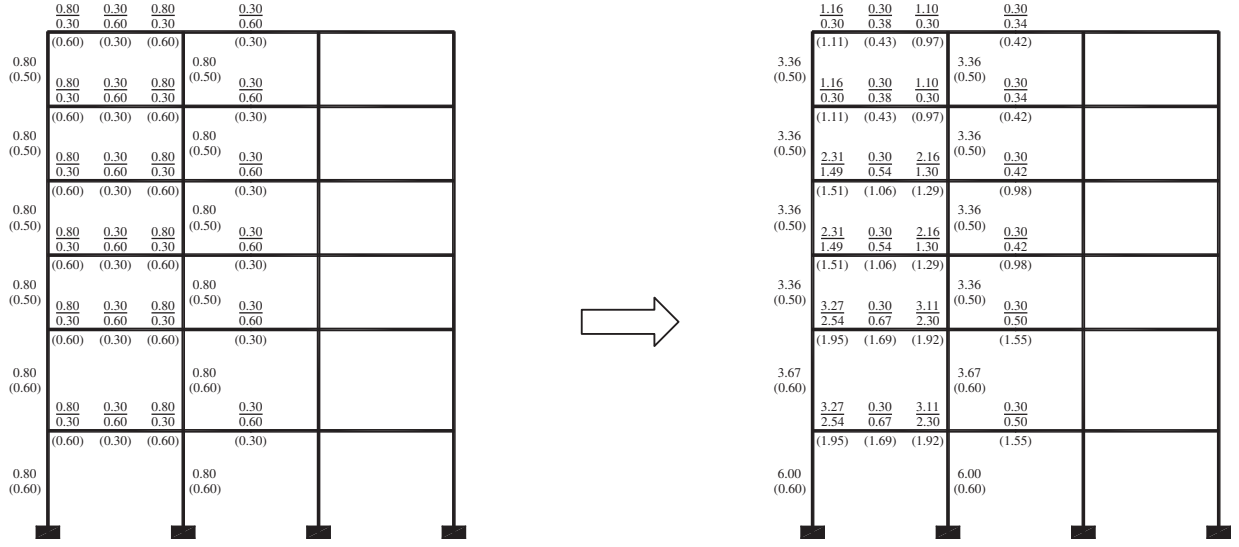

Table 3 (*continued*)

i	$y_{t_d,i}$ (mm) 2	$W_{k,i}$ (N m)	$F_{a,i}$ (N)	$F_{s,i}$ (N)	P_i (N)	$\Delta_{t_d,m}$ (%)	X	λ	$P_{st,i}$ (N)
The second iterative design step									
6	11.13	0.91×10^4	1.64×10^6	-4.15×10^5	1.22×10^6				1.55×10^5
5	19.73	1.67×10^4	1.70×10^6	3.19×10^5	2.02×10^6				2.57×10^5
4	22.07	2.45×10^4	2.22×10^6	1.50×10^5	2.37×10^6	0.348	0.052	0.127	3.02×10^5
3	22.11	2.38×10^4	2.15×10^6	-4.01×10^5	1.75×10^6				2.23×10^5
2	24.03	3.43×10^4	2.86×10^6	7.07×10^5	3.56×10^6				4.54×10^5
1	15.65	0.36×10^4	0.46×10^6	1.48×10^6	1.94×10^6				2.47×10^5

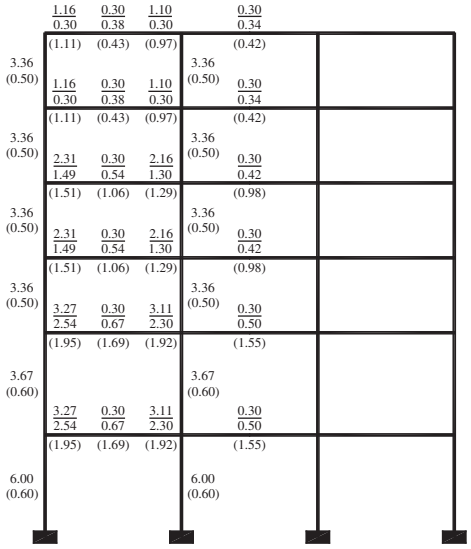

(a) Initial reinforcement ratios (%)

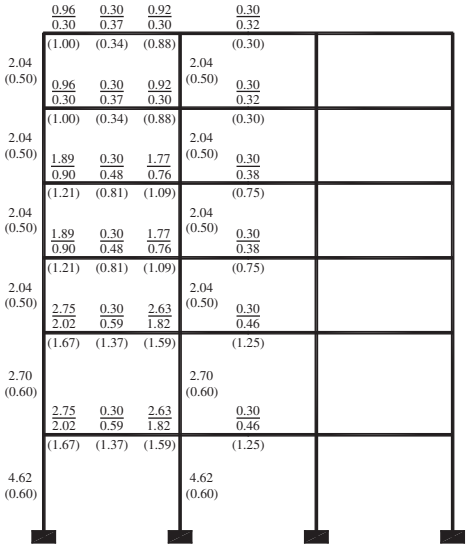

(b) New reinforcement ratios (%)

The third iterative design step

6	10.84	0.78×10^4	1.44×10^6	-4.05×10^5	1.03×10^6				1.37×10^5
5	19.65	1.84×10^4	1.87×10^6	3.35×10^5	2.21×10^6				2.92×10^5
4	21.77	2.19×10^4	2.01×10^6	1.42×10^5	2.15×10^6	0.364	0.055	0.132	2.85×10^5
3	21.58	2.43×10^4	2.25×10^6	-3.71×10^5	1.88×10^6				2.49×10^5
2	23.52	3.33×10^4	2.83×10^6	5.18×10^5	3.35×10^6				4.43×10^5
1	16.36	0.32×10^4	0.39×10^6	1.50×10^6	1.89×10^6				2.50×10^5

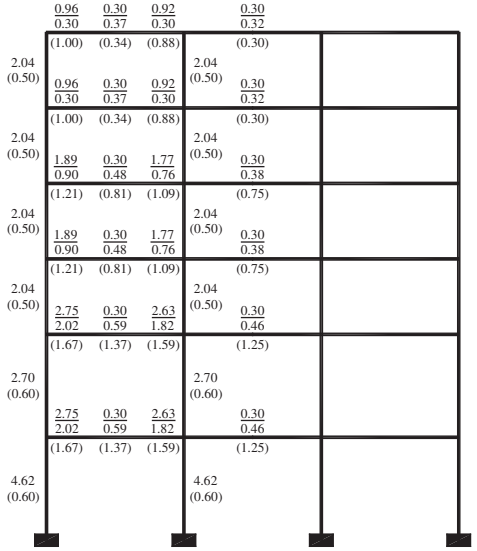

(a) Initial reinforcement ratios (%)

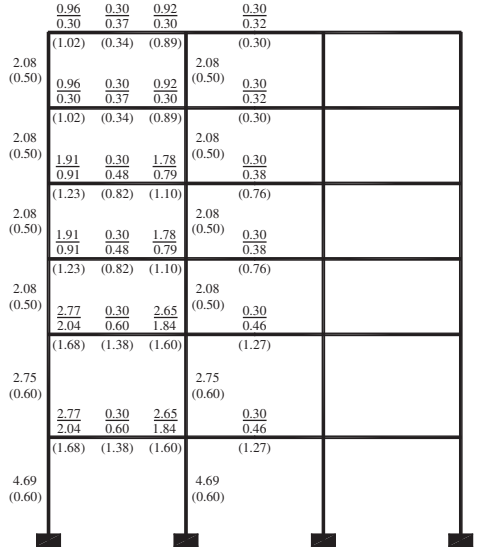

(b) New reinforcement ratios (%) (final design)

Note: The item inside the bracket is the total required area of shear reinforcement per unit length (mm).

Table 4
Design procedures for example II

I	$y_{t_d,i}$ (mm)	$W_{k,i}$ (N m)	$F_{a,i}$ (N)	$F_{s,i}$ (N)	P_i (N)	$\Delta_{t_d,m}$ (%)	X	λ	$P_{st,i}$ (N)
The first iterative design step									
6	9.07	2.94×10^3	6.49×10^5	-2.02×10^5	4.47×10^5				8.88×10^4
5	12.62	2.84×10^3	4.49×10^5	1.05×10^5	5.55×10^5				1.10×10^5
4	14.71	4.52×10^3	6.15×10^5	1.29×10^5	7.44×10^5	0.242	0.088	0.198	1.47×10^5
3	15.02	7.18×10^3	9.56×10^5	-2.64×10^5	6.92×10^5				1.37×10^5
2	17.01	5.80×10^3	6.82×10^5	3.68×10^5	1.05×10^6				2.08×10^5
1	10.90	0.32×10^3	5.96×10^4	6.31×10^5	6.91×10^5				1.37×10^5

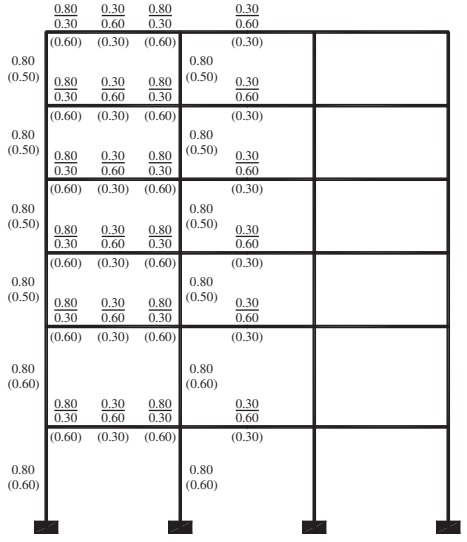

(a) Initial reinforcement ratios (%)

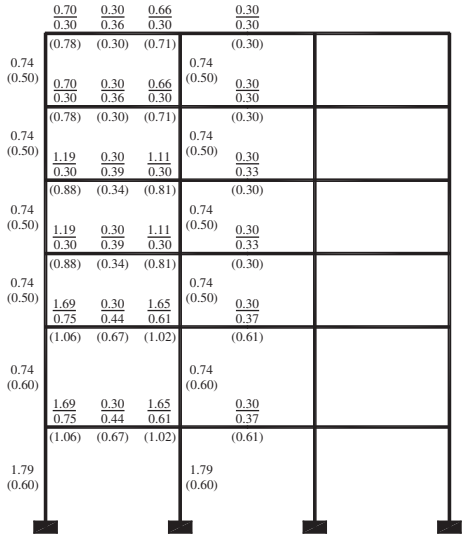

(b) New reinforcement ratios (%)

The second iterative design step									
6	8.94	2.45×10^3	5.48×10^5	-1.97×10^5	3.51×10^5				6.71×10^4
5	12.65	2.37×10^3	3.74×10^5	1.11×10^5	4.85×10^5				9.28×10^4
4	14.78	4.73×10^3	6.40×10^5	1.06×10^5	7.46×10^5	0.233	0.084	0.191	1.43×10^5
3	15.22	7.43×10^3	9.76×10^5	-2.52×10^5	7.24×10^5				1.38×10^5
2	17.10	5.09×10^3	5.96×10^5	4.56×10^5	1.05×10^6				2.01×10^5
1	10.50	0.14×10^3	2.60×10^4	6.48×10^5	6.74×10^5				1.29×10^5

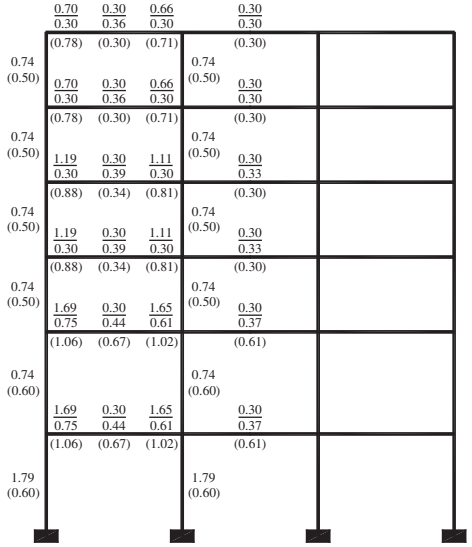

(a) Initial reinforcement ratios (%)

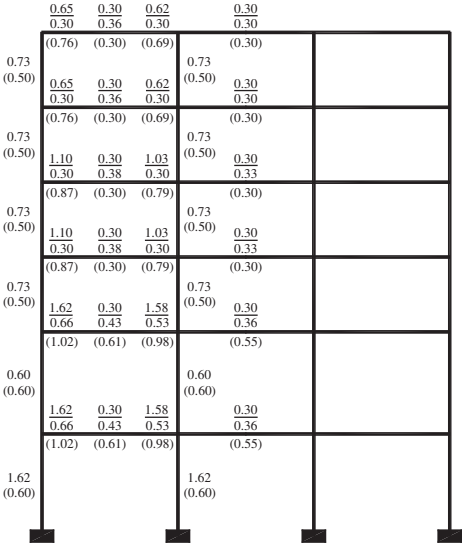

(b) New reinforcement ratios (%)

Table 4 (*continued*)

I	$y_{t_d,i}$ (mm)	$W_{k,i}$ (N m)	$F_{a,i}$ (N)	$F_{s,i}$ (N)	P_i (N)	$\Delta_{t_d,m}$ (%)	X	λ	$P_{st,i}$ (N)
The third iterative design step									
6	8.91	2.43×10^3	5.46×10^5	-1.95×10^5	3.51×10^5				6.79×10^4
5	12.64	2.27×10^3	3.60×10^5	1.12×10^5	4.71×10^5				9.10×10^4
4	14.77	4.71×10^3	6.38×10^5	1.07×10^5	7.45×10^5	0.235	0.085	0.193	1.44×10^5
3	15.16	7.35×10^3	9.70×10^5	-2.57×10^5	7.13×10^5				1.38×10^5
2	17.11	5.56×10^3	6.50×10^5	4.44×10^5	1.09×10^6				2.11×10^5
1	10.60	0.18×10^3	3.54×10^4	6.49×10^5	6.84×10^5				1.32×10^5

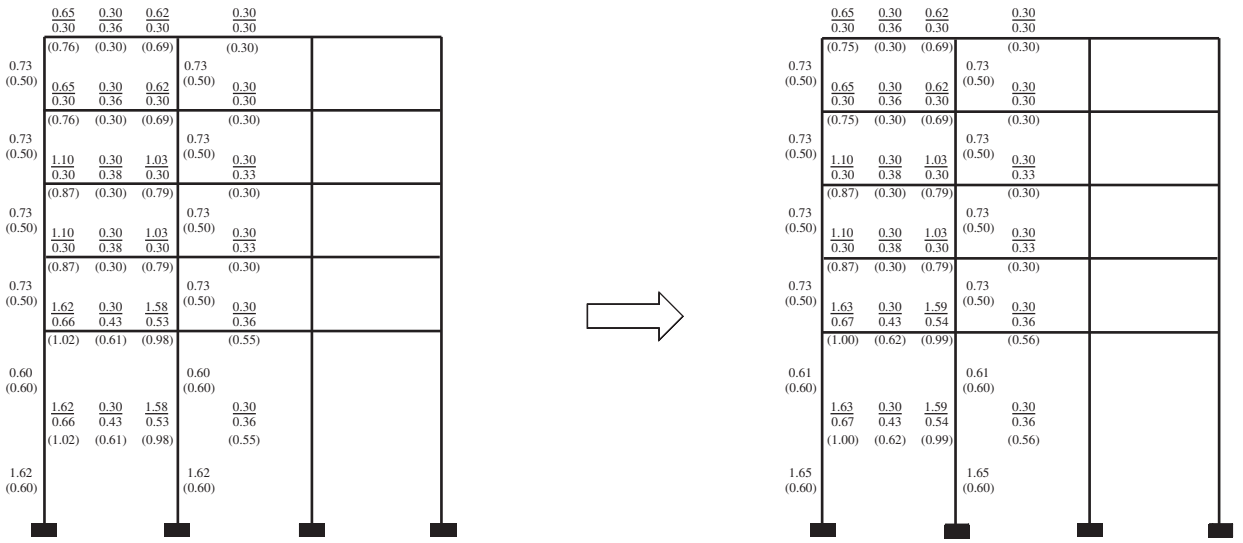

Note: The item inside the bracket is the total required area of shear reinforcement per unit length (mm).

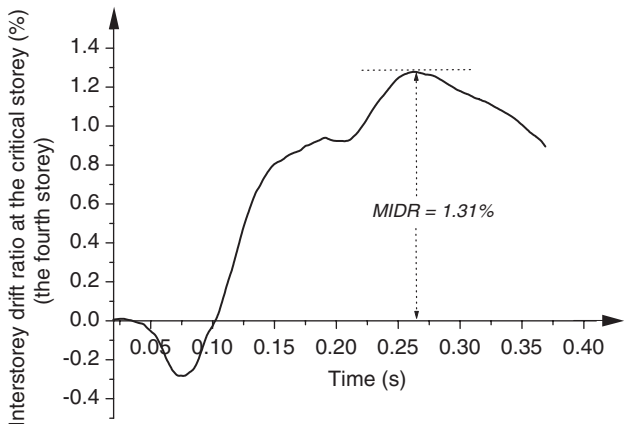

Fig. 7. Responses of the designed frame structure under the given blast force (Example I).

6. Summary and conclusions

A new blast resistant design method has been developed for RC frame structures based on the ESF, which keeps the MIDR under proper control within the expected performance level under given distant surface

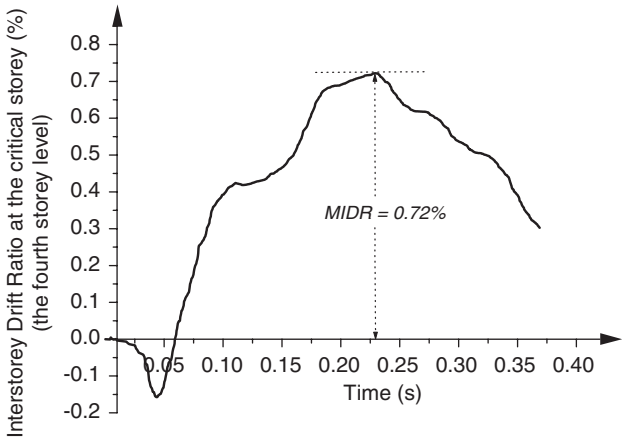

Fig. 8. Responses of the designed frame structure under the given blast force (Example II).

explosions. An equivalent static system is developed for the purpose of simulating the kinetic energy at t_d by the strain energy of additional springs. According to the equilibrium of the equivalent static system, the external static force is obtained. However, this force will produce a larger MIDR demand than that of the frame structure under the blast condition. Thus, the ESF factor λ is introduced to reduce the external static force to finally obtain the ESF.

By comparing the nonlinear dynamic responses of frame structures with corresponding nonlinear static pushover analytical results, a number of sample points of λ are obtained, from which a function of λ is determined with the optimum technique for the closest estimation of these points. It shows the sample points of λ scattered around this optimized function within a straight strip that is bounded between an upper-envelope and a lower-envelope line. The upper-envelope line is utilized in the design for structural safety.

By substituting the ESF with the ultimate strength and the MIDR with the required design target, the calculation model of the ESF has been implemented for the design of a RC frame structure. For given cross-sectional sizes of the frame members, the longitudinal reinforcement ratios are iteratively solved. Two numerical examples show that there is no difficulty in getting computational convergence for the design method based on ESF. However, since the ESF factor is based on the upper-envelope line and the strength hardening of the structure after reaching the ESF, some safety margin is provided as part of the design to control the MIDR responses of the frame structure as indicated from the numerical verifications.

Acknowledgements

This research was supported by a research grant LEO 99.05 provided by the Defence Science & Technology Agency (DSTA), Singapore, under the Protective Technology Research Center, Nanyang Technological University, Singapore. Any opinions, findings and conclusions expressed in this paper are those of the writers and do not necessarily reflect the view of DSTA, Singapore.

References

[1] Bounds WL. Design of blast resistant building in petrochemical facilities. ASCE Task Committee Report on Blast Resistant Design, 1997.

[2] Hyde DW. ConWep: weapons effects calculation program based on technical manual, TM5-855-1. United States Army Engineer Waterways Experiment Station, 1991.

[3] TM 5-855-1. Fundamental of protective design for conventional weapons. Washington, DC: United States Department of the Army; 1986.

[4] Bing Li, Hai-Cheng Rong, Tso-Chien Pan. Drift-controlled design of reinforced concrete frame structures under distant blast conditions, Part I: theoretical basis. International Journal of Impact Engineering, 2006, in press, doi:10.1016/j.ijimpeng.2006.01.010.
[5] ABAQUS. ABAQUS/standard user's manual. HKS, Inc., 2004.
[6] ABAQUS. ABAQUS theory manual. HKS, Inc., 2004.
[7] Hai-Cheng Rong. Performance-based blast resistant design of reinforced concrete frame structures under distant explosions. PhD thesis, Nanyang Technological University, 2005.
[8] Lagarias JC, Reeds JA, Wright MH, Wright PE. Convergence properties of the Nelder–Mead simplex method in low dimensions. SIAM J Optim 1998(9):112–47.
[9] MATLAB. The language of technical computing, version 6.1. The MathWorks, Inc; 2001.
[10] Baker WE, Cox PA, Westine PS, Kulesz JJ, Strehlow RA. Explosion hazards and evaluation. New York: Elsevier Scientific Publishing Company; 1983.
[11] TM5-1300. Structures to resist the effects of accidental explosions, vol. IV, reinforced concrete design. Washington, DC: United States Department of the Army; 1990.
[12] NFEC. Blast resistant structures. Naval facilities engineering command, design manual 2.08. Alexandria, VA: NFEC; 1986.
[13] ETABS. Integrated building design software: concrete frame design manual. Berkeley, CA, USA: Computers and Structures Inc.; 2002.